

Article

Effect of Rotor Thrust on the Average Tower Drag of Downwind Turbines

Shigeo Yoshida ^{1,*}, Kazuyuki Fujii ², Masahiro Hamasaki ¹ and Ao Takada ¹

¹ Research Institute for Applied Mechanics, Kyushu University, 6-1 Kasugakoen, Kasuga, Fukuoka 816-8580, Japan; hamasaki@riam.kyushu-u.ac.jp (M.H.); takada@riam.kyushu-u.ac.jp (A.T.)

² Interdisciplinary Graduate School of Engineering and Science, Kyushu University, 6-1 Kasugakoen, Kasuga, Fukuoka 816-8580, Japan; fujii@riam.kyushu-u.ac.jp

* Correspondence: yoshidas@riam.kyushu-u.ac.jp; Tel. +81-92-583-7747

Received: 28 November 2018; Accepted: 8 January 2019; Published: 12 January 2019



Abstract: A new analysis method to calculate the rotor-induced average tower drag of downwind turbines in the blade element momentum (BEM) method was developed in this study. The method involves two parts: calculation of the wind speed distribution using computational fluid dynamics, with the rotor modeled as a uniform loaded actuator disc, and calculation of the tower drag via the strip theory. The latter calculation considers two parameters, that is, the decrease in wind speed and the pressure gradient caused by the rotor thrust. The present method was validated by a wind tunnel test. Unlike the former BEM, which assumes the tower drag to be constant, the results obtained by the proposed method demonstrate much better agreement with the results of the wind tunnel test, with an accuracy of 30%.

Keywords: wind turbine; downwind; tower shadow; load; tower; BEM; actuator disc

1. Introduction

Horizontal axis wind turbines are categorized as upwind and downwind turbines according to the position of the rotor relative to the tower. Among these, upwind turbines have been predominant throughout the 30 year history of commercial wind turbines. The most essential reason for the unpopularity of the downwind turbines is the presence of a strong aerodynamic interaction between the rotor and the tower, which is commonly known as the “tower shadow effect”. This phenomenon generates impulsive loads and infrasound when one of the blades passes through the wake of the tower [1]. The modeling of the tower shadow effect is a critical technical problem of downwind turbines.

Design loads are calculated on the basis of the international design standard IEC61400-1 [2] or the guidelines for certification bodies DNV GL [3]. In a large number of cases in which the design load is combined with the wind model, the wind turbines can experience failure conditions, as well as various types of wind and marine conditions. The flexibilities of the structure and the controls, in addition to the aerodynamics, hydrodynamics, aero-elastics, and control of the wind turbines, considerably influence the load. The blade element momentum (BEM) method is the most popular tool for determining these characteristics [4,5]. Therefore, the modeling of the tower shadow effect in the BEM is one of the most important technical challenges in the design and development of downwind wind turbines. However, most of the tower shadow models are too simple to express such phenomena, as they consider only the wind speed profile behind an isolated tower [5,6] and not the aerodynamic interaction between the rotor and the tower.

Several studies have been conducted until now that have focused on the variable loads of the downwind turbines caused by the tower shadow effect. Zhao et al. [7] studied the loads on a tower

by performing a comparison between two- and three-bladed upwind and downwind rotors in two different rotor speed conditions using computational fluid dynamics (CFD). The peak to average values of the hub bending moment and the tower base bending moment of the downwind turbine were shown to be 5–6 times and 2.5 times larger, respectively, than those of the upwind turbine. Zahle et al. [8] conducted 2-dimensional CFD analysis for three typical tower concepts of downwind turbines as well as for an upwind turbine; a steep load variation was noted for the downwind turbine, and the implementation of streamlined and four-leg towers was shown to be an effective technique to reduce the load variation caused by the tower shadow effects. Matiz-Chicacausa and Lopez [9] investigated the possibilities of the application of the actuator line model (ALM) to the CFD analysis of the tower shadow effects. The ALM was shown to be useful for load estimation of a downwind turbine under specific conditions.

Although the abovementioned research contributed to the expansion of the understanding of the phenomenon, the authors did not aim to develop models for extensive load calculations based on the design standards and guidelines. Wang and Coton [10] developed a high-resolution tower shadow model for downwind turbines based on the prescribed wake vortex model and an efficient near wake dynamics model of the vorticity trailing the blades. The model demonstrated reasonable agreement with the experimental results, with the exception of the blades passing through the tower wake. However, the load of the tower was not discussed in this research. Yoshida and Kiyoki [11,12] developed the load equivalent tower shadow modeling method. The method considered a bell-shaped wind speed profile behind the tower, which helped obtain the equivalent rotor load variation with the wind turbine CFD analysis. This model was applied to the development of the first multimegawatt-scale commercial downwind turbines, including the SUBARU 80/20 [13] and, later, the Hitachi 2 MW, to realize high performance and safety in complex terrains [14,15]. The technology was extended to the later produced Hitachi 5 MW [16] offshore wind turbines. The model has been successfully applied in engineering applications so far; however, two major problems remained unsolved. The first concern was that the CFD modeling of the rotor–tower configuration required for each operating condition was time-consuming, which made the technique inconvenient for use in the design optimization process. The second issue was that no model was established for the tower shadow effects on the tower drag. Considering the situation, the tower load variation caused by the tower shadow effect was modeled by Yoshida by combining the BEM and the Lifting Line Theory [17]. However, the average tower drag was still not discussed in that research.

Considering these situations, this paper proposes a BEM model for the tower average drag. The formulation is presented in Section 2, and the validation of the method by a wind tunnel test is discussed in Sections 3–5.

2. Methodology

The formulation of the average loads of the towers of the downwind turbine by using the BEM is discussed in this chapter. The following two calculations are considered:

- (1) Wind speed distribution by CFD
- (2) Rotor thrust-induced tower average drag

2.1. Wind Speed Distribution by CFD

The wind speed distribution in front of the rotor is calculated using CFD. Figure 1 shows the top view of the rotor and the tower of a downwind turbine. The tower, which has the diameter D_T , is located in front of the rotor. The free stream wind speed U_0 decreases to $U_0(1 - a)$ at the rotor plane as a result of the rotor thrust. Here, a is the axial induction factor. Figure 2 is the schematic of the CFD involved in the present study. The tower is not included in the model, but the position is termed “virtual tower position” in this research. Further, u_T is the wind speed at the virtual tower position, which is between U_0 and $U_0(1 - a)$, depending on the condition. The rotor is modeled by an actuator

disc model (ADM). The load distribution is assumed to be uniform to realize a convenient application to the BEM. The thrust per unit volume σ of the ADM is as shown in Equation (1):

$$\sigma = \frac{1}{2\pi r w} \frac{dT}{dr} \tag{1}$$

where w is the thickness of the ADM.

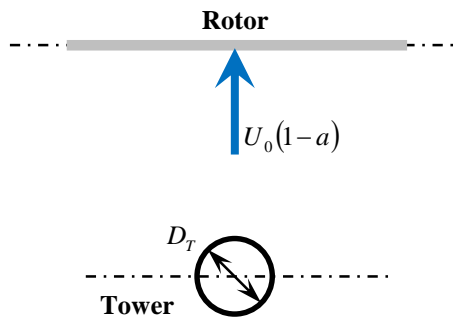


Figure 1. Top view of a downwind turbine. U_0 , free stream wind speed, D_T , tower diameter.

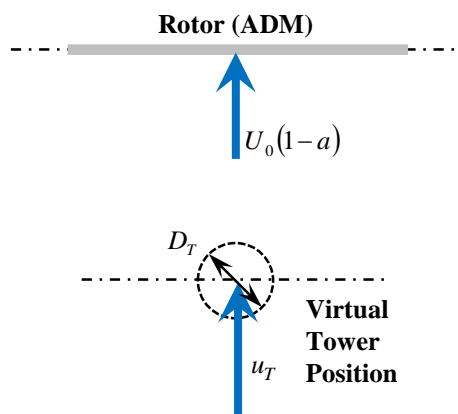


Figure 2. Computational fluid dynamics (CFD) with actuator disc model (ADM). u_T , wind speed at the virtual tower position.

2.2. Rotor Thrust-Induced Tower Average Drag

The wind speed at the tower and the tower drag decrease as the rotor thrust increases due to the aerodynamic interaction. Two factors, that is, the wind speed and the ambient pressure gradient caused by the rotor thrust, are considered in this research. The formulation is based on the assumption of the strip theory, according to which the flow between the sections normal to the tower axis is not taken into account.

(1) Wind Speed Effect

The tower drag decreases proportionally to the square of the wind speed when the tower section drag coefficient remains constant. This influence is modeled herein.

The section drag f_{XT0} of the isolated tower with no rotor interaction is as shown in Equation (2):

$$f_{XT0} = \frac{1}{2} \rho U_0^2 D_T C_{dT0} \quad (2)$$

where C_{dT0} is the drag coefficient at the tower section.

In case the effect of the rotor thrust comes into play, the wind speed at the tower position decreases. Furthermore, the tower section drag also decreases from f_{XT0} to f_{XT} . This is expressed in the following two ways, based on the wind speeds at the free stream and at the virtual tower position, as shown in Equation (3):

$$f_{XT} = \frac{1}{2} \rho U_0^2 D_T C_{dT} = \frac{1}{2} \rho u_T^2 D_T C_{dT0} \quad (3)$$

where C_{dT} is the tower section drag based on the free stream wind speed, and u_T is the wind speed at the virtual tower position, which is calculated by CFD without incorporating a tower model, as explained in the previous section. Here, the drag coefficient C_{dT0} is assumed to be constant as in Equation (2).

Therefore, the tower section drag deviation induced by the rotor thrust Δf_{XT} is calculated as in Equation (4):

$$\Delta f_{XTV} = f_{XT} - f_{XT0} = -\frac{1}{2} \rho U_0^2 D_T C_{dT0} (1 - \mu_T^2) \quad (2)$$

where the normalized wind speed at the virtual tower is

$$\mu_T = \frac{u_T}{U_0}$$

Therefore, the change in the relevant drag coefficient caused by the wind speed change ΔC_{dTV} is calculated by Equation (4), as given in Equation (5):

$$\Delta C_{dTV} = -C_{dT0} (1 - \mu_T^2) \quad (3)$$

This indicates that the term of the tower section drag decreases as the normalized wind speed at the virtual tower, induced by the rotor thrust, decreases.

(2) Effect of the Ambient Pressure Gradient

The tower drag is also dependent on the ambient pressure gradient around the tower. This influence is modeled herein.

The pressure at the virtual tower position p_T is calculated by Bernoulli's law, as in Equation (4):

$$p_0 + \frac{1}{2} \rho U_0^2 = p_T + \frac{1}{2} \rho u_T^2 \quad (4)$$

where p_0 and p_T are the pressures at the free stream and the virtual tower center, respectively. Therefore, the windward pressure gradient $\partial p_T/\partial x_T$ at the virtual tower center is calculated as shown in Equation (5) by the differential of Equation (4):

$$\frac{\partial p_T}{\partial x_T} = -\rho u_T \frac{\partial u_T}{\partial x_T} \quad (5)$$

The section drag by the pressure gradient at the tower section Δf_{XTP} is calculated as in Equation (6) by employing the pressure deviation from the front and back sides of the tower and the tower diameter. The pressure deviation is calculated by the pressure gradient and the windward reference distance Δx_T :

$$\Delta f_{XTP} = \frac{\partial p_T}{\partial x_T} \Delta x_T D_T \quad (6)$$

Assuming a uniform pressure gradient, the tower section drag is expressed as in Equation (7):

$$\Delta f_{XTP} = \int_{-\pi/2}^{\pi/2} \left(\frac{\partial p_T}{\partial x_T} D_T \cos \phi_T \right) \left(\frac{D_T}{2} \cos \phi_T \right) d\phi_T \quad (7)$$

The reference distance is calculated as in Equation (8) using Equations (6) and (7):

$$\Delta x_T = \frac{\pi}{4} D_T \quad (8)$$

Therefore, the change in the tower section drag owing to the pressure gradient is calculated as in Equation (9):

$$\Delta f_{XTP} = \frac{\pi D_T^2 \rho u_T}{4} \frac{\partial u_T}{\partial x_T} = \frac{\pi D_T \rho U_0^2 \mu_T}{4} \frac{\partial \mu_T}{\partial \xi_T} \quad (9)$$

where ξ_T is the normalized distance and can be written as

$$\xi_T = \frac{x_T}{D_T}$$

Therefore, the change in the relevant drag coefficient caused by the pressure gradient ΔC_{dTP} can be written as in Equation (10):

$$\Delta C_{dTP} = \frac{\pi}{2} \mu_T \frac{\partial \mu_T}{\partial \xi_T} \quad (10)$$

This indicates that the term of the tower section drag decreases as the negative pressure gradient caused by the rotor thrust increases.

(3) Total Average Tower Drag

From (1) and (2), the deviation of the drag Δf_{XT} and the drag coefficient ΔC_{dT} induced by the rotor thrust are derived as Equations (11) and (12), respectively:

$$\Delta f_{XT} = \Delta f_{XTV} + \Delta f_{XTP} = \frac{1}{2} \rho U_0^2 D_T \left[-C_{dT0} (1 - \mu_T^2) + \frac{\pi}{2} \mu_T \frac{\partial \mu_T}{\partial \xi_T} \right] \quad (11)$$

$$\Delta C_{dT} = \Delta C_{dTV} + \Delta C_{dTP} = -C_{dT0} (1 - \mu_T^2) + \frac{\pi}{2} \mu_T \frac{\partial \mu_T}{\partial \xi_T} \quad (12)$$

3. Wind Tunnel Test

3.1. Outline

A wind tunnel test for a wind turbine was conducted to validate the theory described in the previous chapter. The rotor–tower interaction was simulated by a dummy tower placed in front of the rotor of the upwind turbine.

3.2. Facility

The Boundary Layer Wind Tunnel at the Research Institute for Applied Mechanics, Kyushu University [18], was used for the test. The wind tunnel has a test section with a width of 3.6 m, a height of 2.0 m, and a length of 15 m. The maximum wind speed is 30 m/s.

3.3. Test Model

The general specifications and the outline of the model and the tower installed in the wind tunnel are presented in Table 1. The blockage ratio, which is the ratio of the rotor area to the cross section of the wind tunnel, is as small as 5.3%. The rotor speed is controlled by the variable dump load. Figure 3 shows the schematic of the test model and the dummy tower. Although the model is an upwind turbine supported by a tower with a diameter of 50.8 mm, a dummy tower is installed in front of the model to mimic the downwind turbine tower. The diameter of the dummy tower is 64 mm, which is 200% the value of the blade chord length. The dummy tower was placed at two positions; $-6D_T$ and $-4D_T$. Figure 4 shows an image of the test model. The dummy tower is shown as located in front of the turbine.

Table 1. Specifications of the test model and the dummy tower.

Item	Specification
Number of blades	2
Rotor diameter D	700 mm
Rotor radius R	350 mm
Tilt angle	0 deg
Coning angles	0 deg
Airfoil	NACA0013
Blade chord length	32 mm
Twist angle	0 deg
Tower diameter D_T	64 mm
Tower position	-338 mm ($-6D_T$) -225 mm ($-4D_T$)

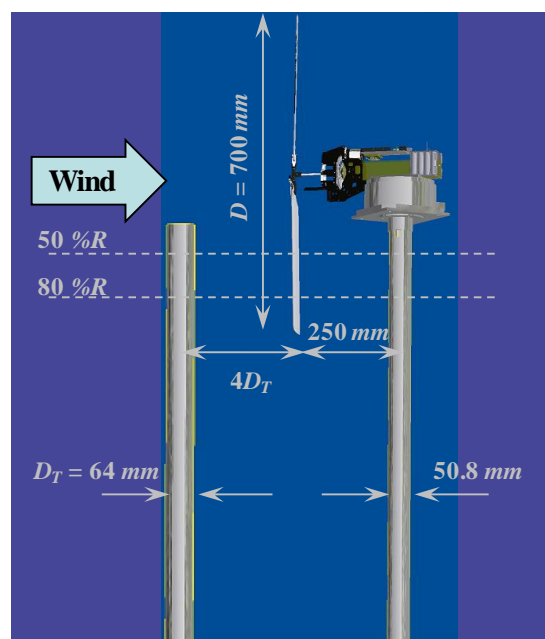


Figure 3. Schematic of the test model (dummy tower at $-4D_T$).



Figure 4. Test model and dummy tower installed in the wind tunnel.

3.4. Measurement

- Rotor speed: Magnetic encoder
- Load (top of the tower): 6-axis Load Cell (Nissho)
- Pressure on the dummy tower (50%R, 80%R, 8 points each): Pressure sensor (Otegiken)

3.5. Test Conditions

- Wind speed (U_0): 6 m/s (uniform, steady)
- Yaw angle: 0 deg
- Blade pitch angle (θ): 4, 6, 8 deg
- Tip speed ratio (λ): 6.6–9.2

3.6. Test Results

The measurements for the power coefficient C_P and the thrust coefficient C_T for the isolated rotor model are shown in Figure 5. The rotor torque was calculated from the rolling moment at the top of the tower. The value of thrust force at the top of the tower was used as the rotor thrust. The maximum value of C_P was noted at approximately $\lambda = 8$ and $\theta = 6$ deg. However, C_T tended to increase with an increase in the tip speed ratio or a decrease in the pitch angle.

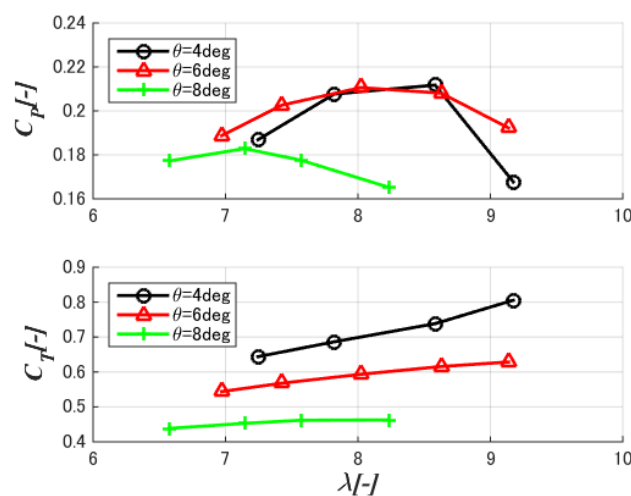


Figure 5. Relationship between the power (C_P) and thrust (C_T) coefficients and the tip speed ratio, λ , blade pitch angle, θ .

The pressure distributions on the dummy tower in typical cases are shown in Figure 6. Here, 0 deg indicates the upwind side of the tower. The pressure on the 50%R was relatively higher than that at 80%R. In general, the pressures around the downwind side of the tower (180 deg) tended to be higher as the rotor thrust was larger.

The details of other characteristics are discussed in Section 5.

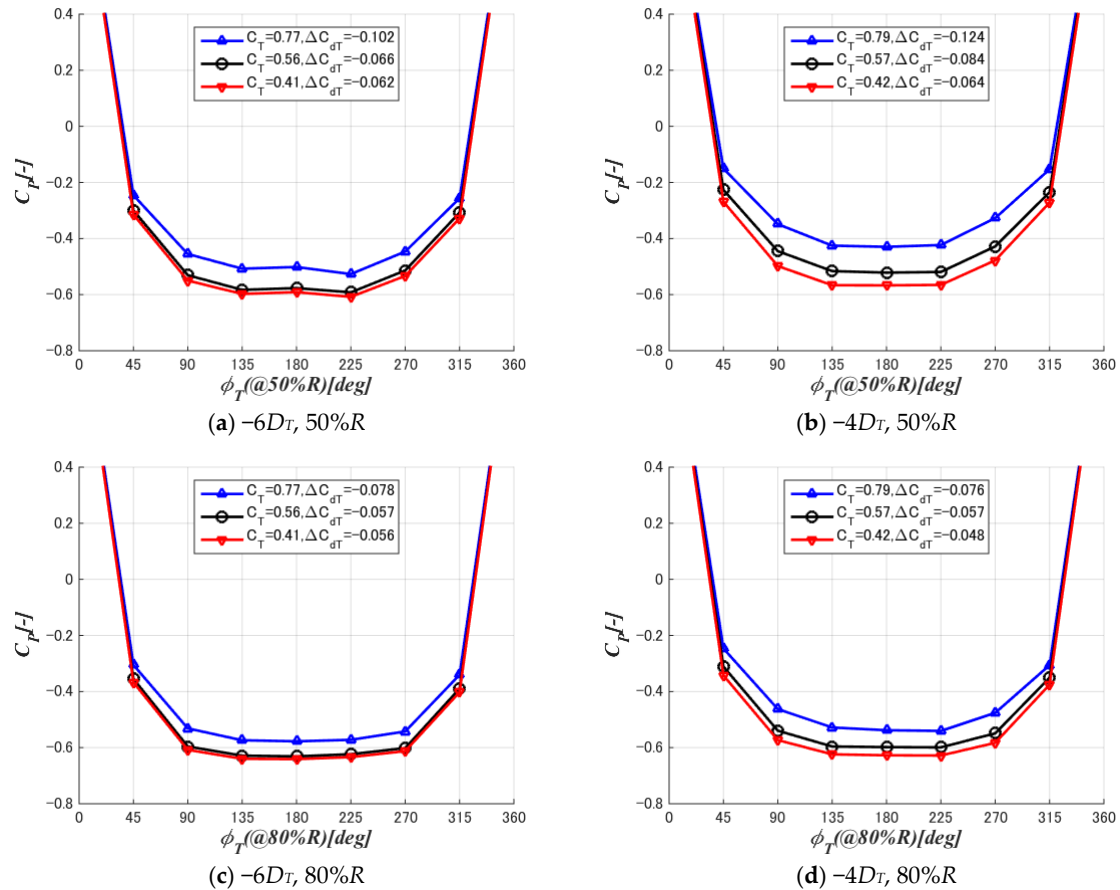


Figure 6. Distribution of the pressure coefficient on the dummy tower in typical cases.

4. Analysis

4.1. Outline

The relationship between the rotor thrust and the tower drag coefficient was determined by the proposed method described in Section 2. The model is generally the same as the one described in Section 3.3; however, the influence of the support was neglected as the support was located far downwind of the rotor, and this distance was fairly large compared to the support's diameter. In addition, the influence of the nacelle was neglected, as it does not affect the outboard sections, as discussed in this study.

4.2. CFD Outline

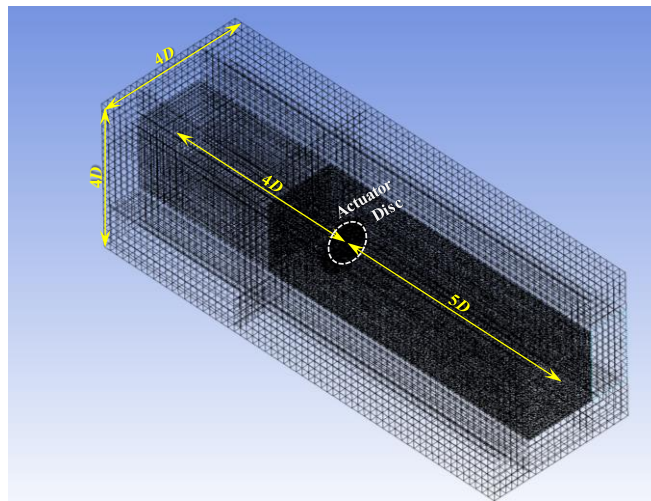
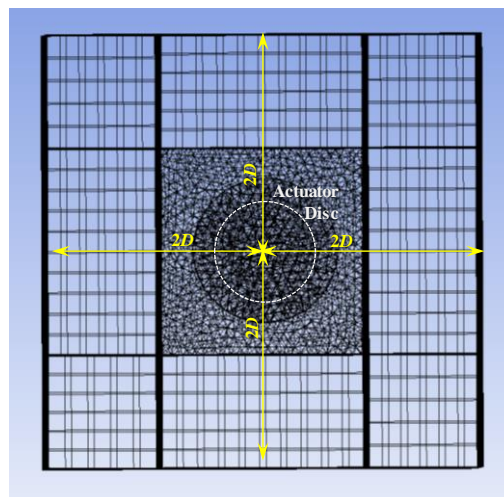
A CFD analysis was conducted for the rotor using ANSYS CFX [19] considering the $k-\omega$ SST turbulence model. The rotor was modeled by an ADM with uniform load distribution.

The simulation domain and the boundary conditions are summarized in Table 2. The model consisted of structured cells around the ADM with y^+ is about 1 and unstructured ones otherwise. The total number of cells was approximately 50 million. The typical cells are shown in Figures 7 and 8.

Table 2. Simulation domain and boundary conditions.

Boundary	Distance from the Rotor Center	Boundary Condition
Rotor	$-D/140 \sim +D/140$	ADM
Tower	Not available	Not available
Inlet	$-4D$	Wind speed (uniform)
Outlet	$+5D$	Ambient pressure
Bottom	$-2D$	Slip
Top	$+2D$	Slip
Side	$-2D, +2D$	Slip

"D": Rotor diameter.

**Figure 7.** CFD domain.**Figure 8.** Cells around the rotor.

4.3. Analysis Conditions

- Wind speed (U_0): 6 m/s (uniform, steady)
- Yaw angle: 0 deg
- Thrust coefficient (C_T): 0.4–0.9 (each 1.0)

4.4. Wind Speed Distributions in Front of the Rotor

The wind speed distributions in typical conditions, $C_T = 0.4$ and 0.9 , are shown in Figures 9 and 10. The circles in these figures denote the positions of the dummy towers at $-6D_T$ and $-4D_T$. The wind speed tended to decrease in front of the tower in general, and the wind speed was lower in the vicinity of the rotor. A comparison between the two conditions shows that the wind speed around the dummy tower decreased as C_T increased. A comparison between the two sections shows that the wind speed in front of the rotor was lower at $50\%R$ compared to that at $80\%R$. The load was uniform on the rotor, and the inboard sections were considerably affected by the rotor.

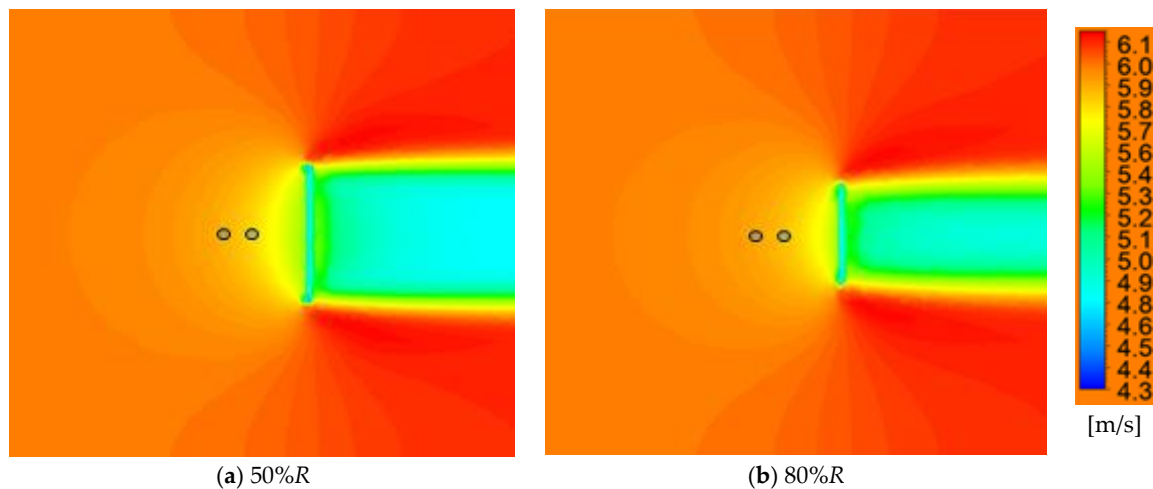


Figure 9. Wind speed distribution in front of the rotor at $C_T = 0.4$, $U_0 = 6$ m/s. (The circles indicate the dummy tower positions at $-6D_T$ and $-4D_T$).

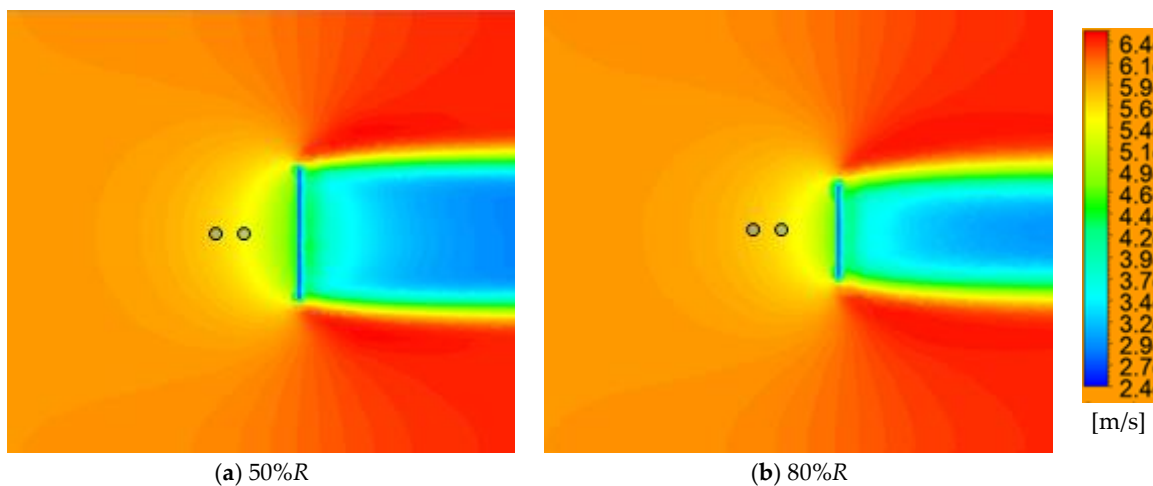


Figure 10. Wind speed distribution in front of the rotor at $C_T = 0.9$, $U_0 = 6$ m/s. (The circles indicate the dummy tower positions at $-6D_T$ and $-4D_T$).

The distributions of the normalized wind speed μ_T and its differential $\partial\mu_T/\partial\zeta_T$ with respect to the normalized distance ζ_T in front of the rotor are shown in Figures 11 and 12. The distributions at $C_T = 0.4$ and 0.9 were identical to those in Figures 9 and 10 in the symmetrical plane. The top subplots correspond to the distributions at $50\%R$, and the bottom ones correspond to those at $80\%R$. The wind speed was lower in the vicinity of the rotor and decreased as the thrust coefficient increased, as mentioned above.

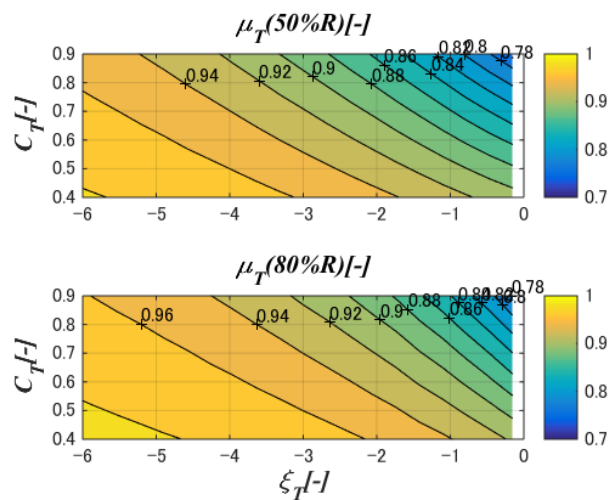


Figure 11. Wind speed in front of the rotor as obtained by CFD. μ_T , normalized wind speed, ξ_T , normalized distance.

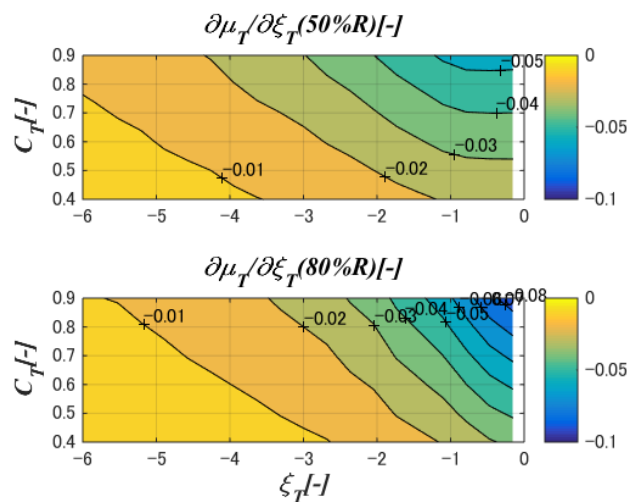


Figure 12. Spatial differential of wind speed in front of the rotor ($\partial\mu_T/\partial\xi_T$) as obtained by CFD.

4.5. Drag Coefficients of the Virtual Tower

The deviation of the drag coefficient of the virtual tower calculated by the present theory is shown in Figure 13. The x -axis denotes the virtual tower position, and the y -axis denotes the thrust coefficient. The diameter of the tower D_T was assumed to be 64 mm, as in the experiment. As indicated by Figures 11 and 12, the drag coefficient tended to be smaller as the rotor–tower clearance decreased and the thrust coefficient increased. The drag tended to be smaller at 50%R than at 80%R.

As shown in Equation (14), the rotor thrust-induced tower drag deviation consisted of the wind speed term and the pressure gradient term. Figure 14 shows the share of the wind speed term to the total deviation. It indicates that approximately 80% of the change in the drag was caused by the first term of Equation (12), i.e., the decrease in the wind speed, rather than the pressure gradient.

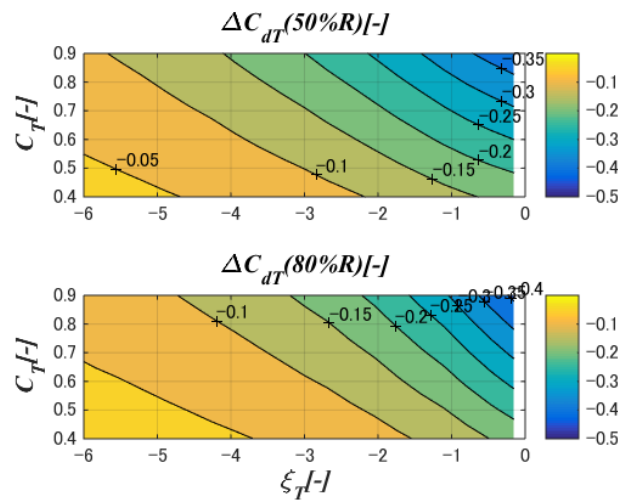


Figure 13. Relationship between the tower section drag and rotor thrust and the virtual tower position. ΔC_{dT} , drag coefficient.

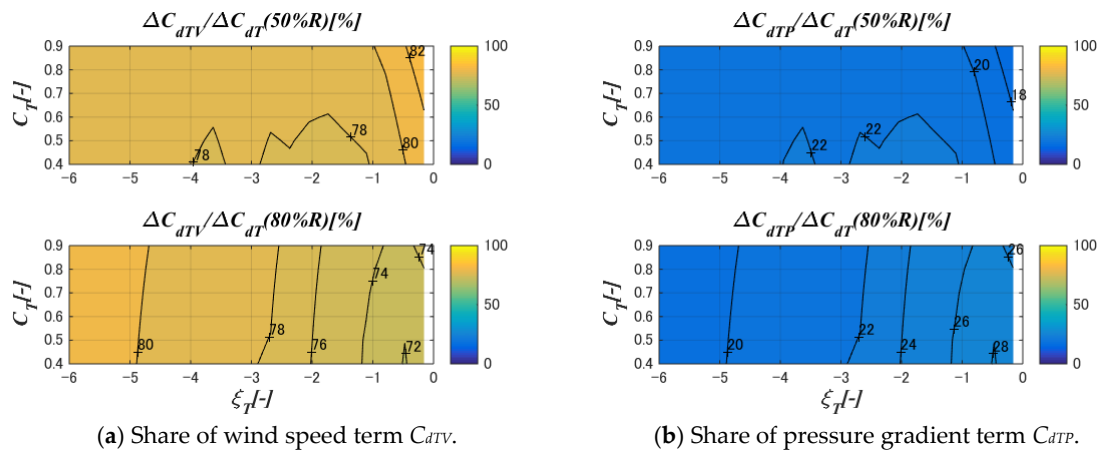


Figure 14. Share of the wind speed term C_{dTV} in the total C_{dT} tower section drag coefficient.

5. Validation

The thrust-induced drag deviations ΔC_{dT} to the thrust coefficient at $-6D_T$ and $-4D_T$ are shown in Figure 15. The lines are approximations for which the intercepts are at $\Delta C_{dT} = 0$ and $C_T = 0$ by definition. The ΔC_{dT} values for all the cases are shown to be almost proportional to C_T . The proportion factors are summarized in Table 3. The factors of the former BEM are zero, as the method does not consider the influence of the rotor thrust on the tower drag. On the other hand, the proposed method shows good agreement with the test. The drag coefficients tended to decrease as the rotor thrust increased. The drag coefficient at the 50%R section was smaller than at the 80%R section. Further, the drag coefficient decreased as the tower was placed closer to the rotor.

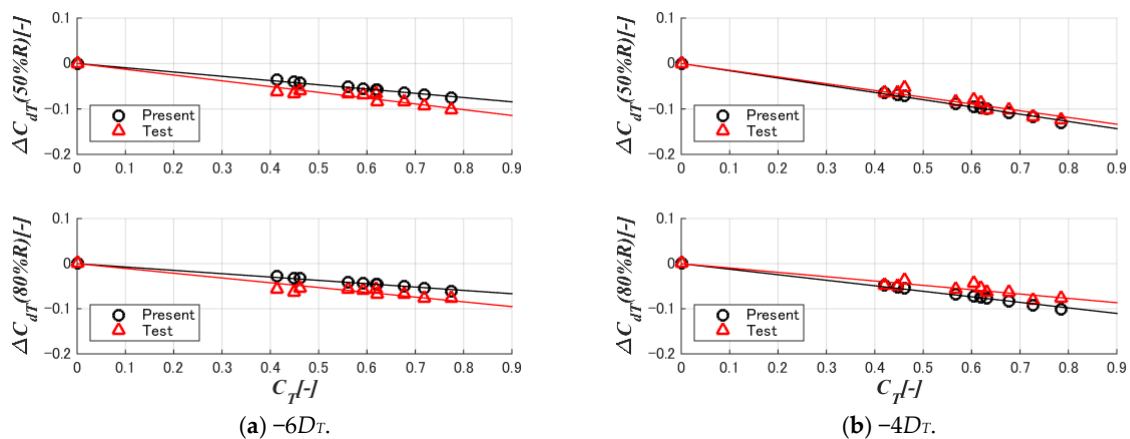


Figure 15. Relationship between tower drag and rotor thrust.

Table 3. Fraction of the deviation of the tower drag coefficient to the thrust coefficient.

Dummy Tower Position	Tower Section	Test		Present
		$\Delta C_{dT}/C_T$ [-]	$\Delta C_{dT}/C_T$ [-]	Deviation from the Test
-6D _T	50%R	-0.1270	-0.0937	-26.2%
	80%R	-0.1058	-0.0741	-30.0%
-4D _T	50%R	-0.1484	-0.1594	+7.4%
	80%R	-0.0961	-0.1225	+27.5%

6. Conclusions

A novel analysis method to calculate the average tower drag of downwind turbines, which considers the rotor-induced average tower drag coefficient, was developed. It consists of two terms, that is, the decrease in the wind speed and the pressure gradient caused by the rotor thrust. The rotor thrust distribution is assumed to be uniform. The method was validated by a wind tunnel test. Unlike the former blade element momentum (BEM) method, which assumes the tower drag to be constant, the proposed method demonstrates a much better agreement with the wind tunnel test, with an accuracy of up to 30%. The results show that the tower drag decreases proportionally to the rotor thrust. With regard to the sensitivity of the tower drag with respect to the rotor thrust, the following characteristics were noted:

- The drag coefficient was larger in the inboard section (50%R) than in the outboard section (80%R).
- The drag coefficient decreased as the tower was positioned closer to the rotor.
- Of the two terms influencing the deviation of the tower section drag, the effect of the decrease in wind speed was more dominant in leading to the decrease in the tower section drag.

By preparing the database of the relationship between the rotor thrust coefficient for the wind speed distribution in front of the rotor, the proposed method is expected to improve the accuracy of the load calculation in the BEM.

In future studies, the present model is planned to be extended to variable loads of wind turbine blades in succession.

Author Contributions: S.Y. organized the research, formulation, and validation. K.F. conducted the computational fluid dynamics simulations, and M.H. and A.T. conducted the wind tunnel test.

Funding: The wind tunnel test was conducted with funding from the “Advanced Practical Research and Development of Wind Power Generation/Advanced Practical Development of Wind Turbine Components/Research on Over 10 MW Class Wind Turbines (Whole Design)” of the New Energy and Industrial Technology Development Organization (NEDO) in 2013–2014.

Acknowledgments: The authors express gratitude to Keiji Matsushima, Kimihiko Watanabe, and Yuji Ohya for their support for the wind tunnel test. The authors would also like to thank Masataka Motoyama and Omar Ibrahim for their support in the computational fluid dynamics simulation.

Conflicts of Interest: The authors declare no conflicts of interest.

Nomenclature

C_{dT}	Tower drag coefficient
C_{dT0}	Tower drag coefficient with no rotor thrust
C_P	Power coefficient
C_p	Pressure coefficient of the tower
C_T	Thrust coefficient
D	Rotor diameter
D_T	Tower diameter
f_{XT}	Tower section drag
f_{XT0}	Tower section drag with no rotor thrust
p_0	Free stream pressure
p_T	Pressure at the tower position
R	Rotor radius
r	Station radius of the blade element
T	Rotor thrust
U_0	Free stream wind speed
u_T	Wind speed at the tower position
w	Thickness of the actuator disc
T	Longitudinal (or windward) position
C_{dT}	Deviation of the tower drag coefficient from that of the isolated tower
ΔC_{dTP}	Deviation of the tower drag coefficient by the effect of the pressure gradient
ΔC_{dTV}	Deviation of the tower drag coefficient by the wind speed
Δf_{XT}	Deviation of the tower section drag from that of the isolated tower
Δf_{XTP}	Deviation of the tower section drag by the effect of the pressure gradient
Δf_{XTV}	Deviation of the tower section drag by the wind speed
θ	Blade pitch angle
λ	Tip speed ratio
μ_T	Normalized wind speed at the tower position
ζ_T	Position normalized by the tower diameter
ρ	Air density
ϕ_T	Azimuth position around the tower (0 deg in front, clockwise around the vertical axis)
ADM	Actuator disc model
ALM	Actuator line model
BEM	Blade element momentum (method)
CFD	Computational fluid dynamics

References

1. Gipe, P. *Wind Energy Comes of Age*; John Wiley and Sons: Chichester, UK, 1995.
2. *Wind Turbines—Part 1: Design Requirements*; IEC61400-1, Ed. 3; International Electrotechnical Commission: Geneva, Switzerland, 2005.
3. Germanischer Lloyd. *Guidelines for the Certifications of Wind Turbines, Edition 2010*; Germanischer Lloyd: Hamburg, Germany, 2010.
4. Burton, T.; Jenkins, N.; Srpe, D.; Bossanyi, E. *Wind Energy Handbook*, 2nd ed.; John Wiley and Sons: Chichester, UK, 2011.
5. Jonkman, J.M.; Buhl, M.L., Jr. *FAST User's Guide*; NREL/TP-500-38230; NREL: Golden CO, USA, 2005.
6. DNV GL. *Bladed, Version 4.7*; DNV GL: Bristol, UK, 2016.
7. Zhao, Q.; Sheng, C.; Afjeh, A. Computational aerodynamic analysis of offshore upwind and downwind turbines. *J. Aerodyn.* **2014**, *2014*, 860637. [[CrossRef](#)]

8. Zahle, F.; Madsen, H.A.; Sorensen, N.N. Evaluation of Tower Shadow Effects on Various Wind Turbine Concepts. Available online: <http://orbit.dtu.dk/files/3550506/ris-r-1698.pdf> (accessed on 19 July 2018).
9. Matiz-Chicacausa, A.; Lopez, O.D. Full downwind turbine simulations using actuator line method. *Model. Simul. Eng.* **2018**, *2018*, 2536897. [[CrossRef](#)]
10. Wang, T.; Coton, F.N. A high resolution tower shadow model for downwind wind turbines. *J. Wind Eng. Ind. Aerodyn.* **2001**, *89*, 873–892. [[CrossRef](#)]
11. Yoshida, S.; Kiyoki, S. Load equivalent tower shadow modeling for downwind turbines. *J. JSME* **2007**, *37*, 1273–1279. [[CrossRef](#)]
12. Yoshida, S.; Kiyoki, S. Load equivalent tower shadow modeling. In Proceedings of the European Wind Energy Conference 2007, Milano, Italy, 7–10 May 2007.
13. Nagao, T.; Kato, T.; Shiraishi, T.; Yoshida, S.; Sugino, J. Development of advanced wind turbine systems for remote islands. *Wind Eng.* **2006**, *28*, 729–740. [[CrossRef](#)]
14. Yoshida, S. Performance of downwind turbines in complex terrains. *Wind Eng.* **2006**, *30*, 487–501. [[CrossRef](#)]
15. Yoshida, S. *Nacelle Yaw Measurement of Downwind Turbines in Complex Terrains*; Windtech International: Groningen, The Netherlands, 2008.
16. Saeki, M.; Sano, T.; Kato, H.; Owada, M.; Yoshida, S. Concept of the HITACHI 5MW offshore downwind turbine. In Proceedings of the European Wind Energy Conference 2014, Barcelona, Spain, 10–13 March 2014.
17. Yoshida, S. Combined blade-element momentum—Lifting line model for variable loads of downwind turbine towers. *Energies* **2018**, *11*, 2521. [[CrossRef](#)]
18. Research Institute of Applied Mechanics, Kyushu University, Boundary Layer Wind Tunnel. Available online: https://www.riam.kyushu-u.ac.jp/windeng/en_equipment.html (accessed on 10 November 2018).
19. ANSYS. *ANSYS CFX*; ANSYS: Canonsburg, PA, USA, 2006.



© 2019 by the authors. Licensee MDPI, Basel, Switzerland. This article is an open access article distributed under the terms and conditions of the Creative Commons Attribution (CC BY) license (<http://creativecommons.org/licenses/by/4.0/>).